ACS Energy LETTERS

http://pubs.acs.org/journal/aelccp

LETTER

Synergistic Degradation Mechanism in Single Crystal Ni-Rich NMC//Graphite Cells

Galo J. Páez Fajardo,* Eleni Fiamegkou, James A. Gott, Heng Wang, Israel Temprano, Ieuan D. Seymour, Matthew J. W. Ogley, Ashok S. Menon, Ifan E. L. Stephens, Muhammad Ans, Tien-Lin Lee, Pardeep K. Thakur, Wesley M. Dose, Michaël F. L. De Volder, Clare P. Grey, and Louis F. J. Piper*

Cite This: *ACS Energy Lett.* 2023, 8, 5025−5031

Read Online

ACCESS | Metrics & More | Article Recommendations | Supporting Information

ABSTRACT: **Oxygen loss at high voltages in Ni-rich NMC//graphite Li-ion batteries promotes degradation, but increasing evidence from full cells reveals that the depth of discharge choice can further accelerate aging, i.e., synergistic degradation. In this Letter, we employ cycling protocols to examine the origin of the synergistic degradation for single crystal Ni-rich NMC//graphite pouch cells. In regimes where oxygen loss is not promoted (V < 4.3 V), a lower cutoff voltage does not affect capacity retention (after 100 cycles), despite significant graphite expansion occurring. In contrast, when NMC surface oxygen loss is induced (V > 4.3 V), deeper depth of discharge leads to pronounced faster aging. Using a combination of post-mortem analysis and density functional theory, we present a mechanistic description of surface phase densification and evolution as a function of voltage and cycling. The detrimental impact of this mechanism on lithium-ion kinetics is used to explain the observed cycling results.**

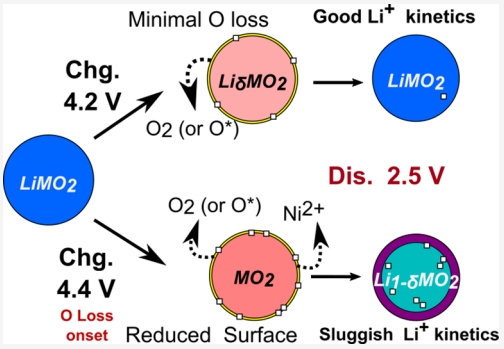

The study of degradation mechanisms for Li-(Ni,Mn,Co)O_2 or NMC cathodes at high voltages and state of delithiation is an active area of research,[1−7] which is important for assisting the electrification of the transport sector.[8] The degradation rate varies with the Ni content in NMC,[9−11] operational voltage windows,[4,12] and particle morphology, i.e., polycrystalline (PC) vs single crystal (SC).[13] In principle, an optimal choice of these three features (SC, Ni ≈ 50%, 3.0−4.3 V) can lead to long-term cell stability to power an electric vehicle for over 1.6 million kilometers.[13]

Realizing even higher energy density applications requires increasing both cell longevity (long-term capacity retention) and specific capacity, i.e., higher Ni contents (Ni > 60%) and wider voltage windows. Most studies to date focus on understanding oxygen loss induced degradation at high voltage, often in half coin cell configurations.[5,14] However, increasing evidence suggests considering both low and high voltage cutoffs for degradation studies when focusing on full cells. For example, Dahn et al.[4] show a steady performance of SC Ni-rich systems (Ni ≈ 80%) with adjustments to the (3.0−4.2 V) voltage window, i.e., avoiding degradation at both voltages limits. Meanwhile, Dose et al.[3] studied degradation in PC NMC811//graphite cells in a wider voltage window (2.5−4.3 V), observing faster degradation when cycling in the full voltage window (with less time spent at high voltages) compared to high voltage holds or cycling. These studies suggest a *synergistic* mechanism between the low and high voltage degradation modes in full cells. Our previous work showed that low voltage degradation related to sluggish Li-ion diffusion[15] in cells cycled with a 2.5−4.2 V window could be overcome by improving the lithium reinsertion kinetics into NMC.[16] However, the relationship between the low and high voltage modes, leading to synergistic degradation, is still elusive and has motivated this study.

In this Letter, we investigate the underlying mechanism of the synergistic degradation in terms of cathode and anode evolution by employing SC Ni-rich NMC//graphite pouch cells as a model system under different cycling conditions. Tailoring the cycling voltage window allows us to isolate degradation mechanism(s) at low and high voltages. We employ post-mortem X-ray and microscopy studies and density functional theory at the material level to interpret the

Received: August 3, 2023
Revised: October 20, 2023
Accepted: October 26, 2023
Published: November 6, 2023

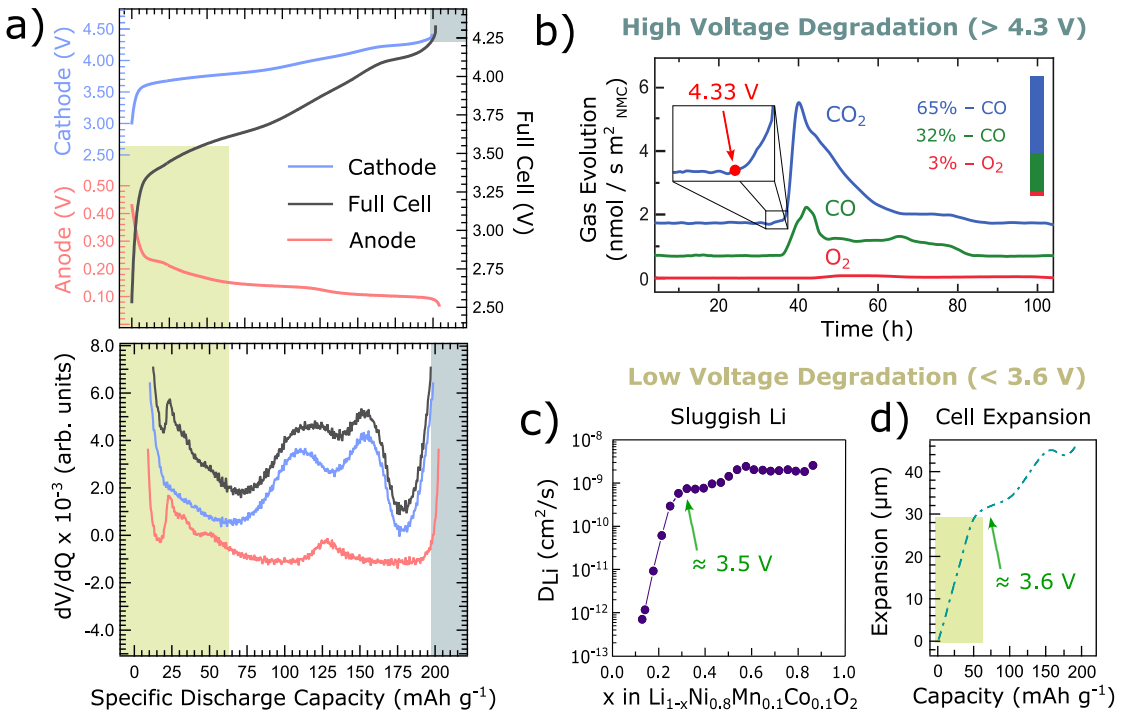

Figure 1. (a) Electrochemical profiles measured in a Ni-rich NMC//lithium foil//graphite three-electrode cell during discharge with a 2.5−4.4 V potential window. d*V*/d*Q* analysis highlights the individual contributions of the anode and cathode to the full cell profile. Highlighting in (a) indicates the high and low voltage degradation mechanisms. High Voltage: (b) OEMS gas evolution (CO_2 − oxygen loss byproduct) showing the oxygen loss voltage threshold at 4.33 V vs Li/Li$^+$. Low Voltage: (d) Electrochemical dilatometry of a pouch cell during discharge indicating cell expansion as a function of capacity. (c) GITT measurements reveal the Ni-rich cathode developing an exponential reduction of Li-ion diffusion (sluggish Li). GITT measurement figure was reproduced from ref 15. Copyright 2019 American Chemical Society.

electrochemical data. Details of the pouch cells (402035-S204070C), electrodes, materials, and experimental details are provided in the Supporting Information.

Combined findings from electrochemical analysis and coupled characterization, i.e., online mass spectrometry and dilatometry, are used to identify the critical low and high voltage regimes (Figure 1). At low voltages, the sudden decrease in the diffusion of lithium ions in Ni-rich oxide lattice (Figure 1c) is an intrinsic material property, which depends on the degree of relithiation during the discharging stage.[15,17] The reinsertion low-voltage Li diffusion drop leads to a first-cycle capacity loss[15] and could influence cathode reinsertion kinetics in the long term.[16] At high voltages, online electrochemical mass spectrometry (OEMS) studies of the Ni-rich cathode show that the onset potential for oxygen-loss-related gas evolution is 4.33 V vs Li/Li$^+$, in accordance with the literature.[6,18,19] Results from cell dilatometry shown in Figure 1d indicate that anode expansion can be active at both low and high voltages, but more rapid changes occur below 3.6 V.[20] Overall, we have identified 4.3 and 3.6 V vs graphite as high and low voltage cutoffs of interest for degradation.

As a result, we employed four cycling protocols to examine the individual and synergistic degradation modes. Restricted (3.6−4.2 V) is the reference protocol where neither low nor high voltage degradation will affect capacity performance. High Voltage (3.6−4.4 V) tests the effects of cycling beyond the oxygen loss threshold, while Standard (2.5−4.2 V) assesses the capacity retention effects of the low voltage mechanisms only. Full Window (2.5−4.4 V) combines both ends and is anticipated to exhibit accelerated fade. Experiments are performed at 40 °C based on previous studies of the same cells,[16,21] where higher cycling temperature improved the lithium reinsertion kinetics into the NMC bulk and overcome the low-voltage sluggish Li-ion bulk diffusion when cycled below the oxygen loss onset.

Figure 2 summarizes the capacity retention of cells cycled with the Restricted, High Voltage, Standard, and Full Window cycling protocols over 100 C/3 cycles following formation cycles; refer to Supporting Information for details. Increasing the lower-cutoff voltage (LCV) from 2.5 V (Standard) to 3.6 V

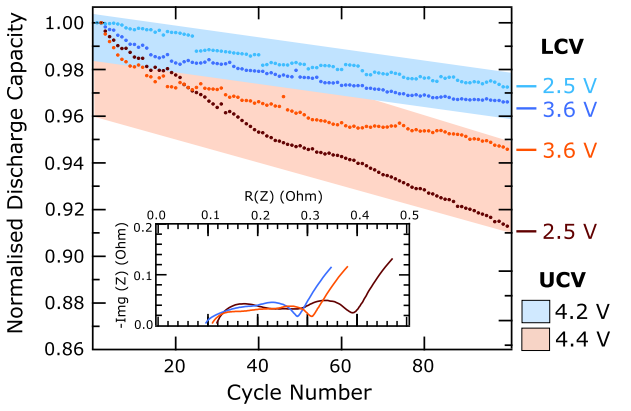

Figure 2. Capacity retention with increasing number of cycles. 4.2 V UCV degradation is SEI dominated, and 4.4 V UCV is the accelerated degradation regime. Inset: EIS studies at 3.8 V after 100 cycles showing impedance evolution as a function of the cell cycling conditions. The Full Window cycling protocol leads to synergistic degradation in both capacity retention and increased impedance arcs.

https://doi.org/10.1021/acsenergylett.3c01596
ACS Energy Lett. 2023, 8, 5025−5031

(Restricted) with a 4.2 V UCV reduced the initial specific capacity from 191.7 to 123.3 mAh/g (Figure S1). Below the oxygen loss, the depth of discharge (DoD) has minimal impact on capacity retention over 100 cycles, i.e., a 0.64% difference between the Restricted (96.61%) and Standard (97.25%) cycling protocols. Numerical analysis in section S2 and Figure S2 supports a SEI dominated degradation mechanism. The slight difference has been attributed to faster SEI growth with a 3.6 V DoD.[4,22] In addition, C/20 diagnostic cycling, in Table 1, recovers almost all the capacity loss, i.e, kinetically limited.

Table 1. Specific Capacity (mAh/g) from the Second Cycle of the Respective C/20 Diagnostic Cycles (after 100 C/3 Cycles) in the UCV Regime with No Oxygen Loss (i.e., UCV < 4.3 V) and with Oxygen Loss (i.e., UCV > 4.3 V)

Below Oxygen Loss	
	C/20: 2.5−4.2 V
100 cycles at	After 100 C/3 cycles
C/3: 3.6−4.2 V	198.792 mAh/g
C/3: 2.5−4.2 V	199.502 mAh/g
Above Oxygen Loss	
	C/20: 2.5−4.4 V
100 cycles at	After 100 C/3 cycles
C/3: 3.6−4.4 V	205.493 mAh/g
C/3: 2.5−4.4 V	197.954 mAh/g

As a result, the additional graphite expansion does not contribute significantly to capacity fade at these C-rates.

Comparing the Restricted and the High Voltage cycling protocols shines light on the extent of the accelerated capacity decay when charging to high voltage. Increasing the UCV to 4.4 V with a 3.6 V LCV (Figure S1) adds 10.8 mAh/g specific discharge capacity to the first cycle (134.1 mAh/g for High Voltage) and decreases the capacity retention by 2.02% after 100 cycles (from 96.61% to 94.59%, respectively). By further increasing the DoD and accessing both the low and high voltage regimes, the Full Window protocol in Figure 2 shows the fastest rate of degradation (at C/3 and C/20 charge rates) with a capacity retention of 91.29−5.32% lower than the Restricted protocol after 100 cycles. Additionally, similar numerical studies for the SEI-driven capacity fade in section S2 confirm that the Full Window degradation cannot be described as solely SEI driven. Compared to the Restricted protocol, the capacity loss with coupled low and high voltage degradation is greater (5.32%) than the sum of the low voltage only (0.64% between Restricted and Standard) and high voltage only (2.02% between Restricted and High Voltage). This is evidence of synergistic degradation.

The corresponding EIS data after cycling provide additional evidence of synergistic degradation. The inset in Figure 2 shows a shift of the arc at low frequencies (charge transfer, R_{CT}) which stands orders of magnitude lower compared to their PC counterparts.[3] The arc starts at 0.28 Ω and ends at 0.39 Ω for the Full Window cycling protocol and evolves with the cycling protocols (Restricted < High Voltage < Full Window). Namely, the arc maximum value is at 0.23 Ω for the Restricted cycling protocol and shifts to 0.28 Ω and 0.34 Ω for the High Voltage and Full Window protocol, respectively.

The changes in the differential capacity, dQ/dV curves (Figure 3) of the High Voltage and Full Window cycling protocols, give information on the Ni-rich NMC phase transitions. Decaying dQ/dV signal for the peak labeled P_4 in Figure 3a has been linked with the structural H2/H3 phase transition.[23,24] However, with the ongoing debate about the presence of this transition in Ni-rich materials,[17,21,25] the P_4 peak can rather be directly associated with electrochemical evolution of the c lattice parameter (dc/dV where V is the voltage).[26] If $P_4 \rightarrow 0$, dc/d$V \rightarrow 0$ also, which translates into a less responsive c lattice parameter during cycling.

This peak is invariant over 100 cycles, with the Restricted (Figure S3) and the High Voltage (Figure 3a) cycling protocols implying an active c lattice parameter and suggesting that the formation of oxygen vacancies does not propagate into the bulk. This means that surface degradation pathways account for the gradually increasing EIS arcs between the

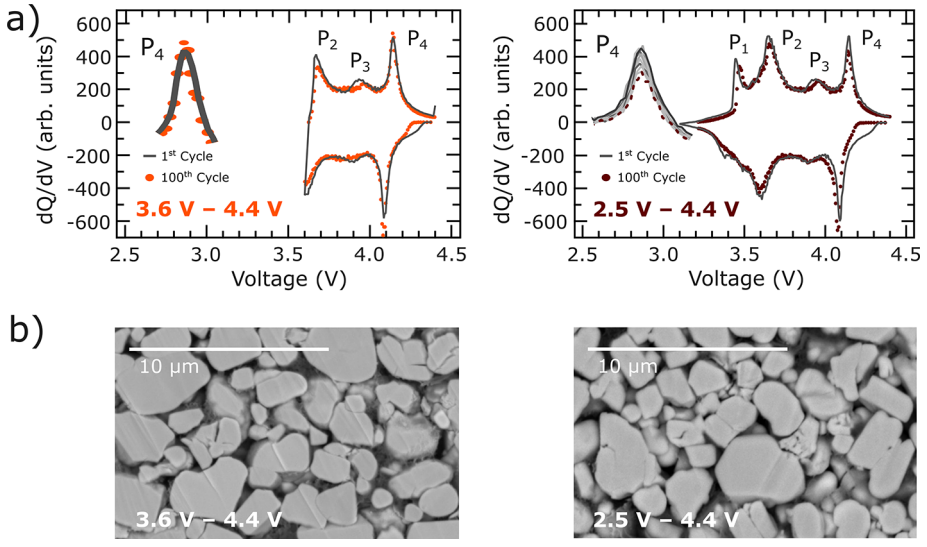

Figure 3. (a) dQ/dV between cycle 1 (line) and after 100 cycles (solid dots) comparing structural changes from the Full window (right) and High voltage (left) cycling protocols via the P_4 peak evolution. Inset includes gradual P_4 changes correspond to cycle numbers 1, 10, 20, ..., 90, and 100. (b) Cross-section BSE SEM images of the cathode electrode after 100 cycles. The Ni-rich NMC particles show no sign of microcracking.

https://doi.org/10.1021/acsenergylett.3c01596
ACS Energy Lett. 2023, 8, 5025−5031

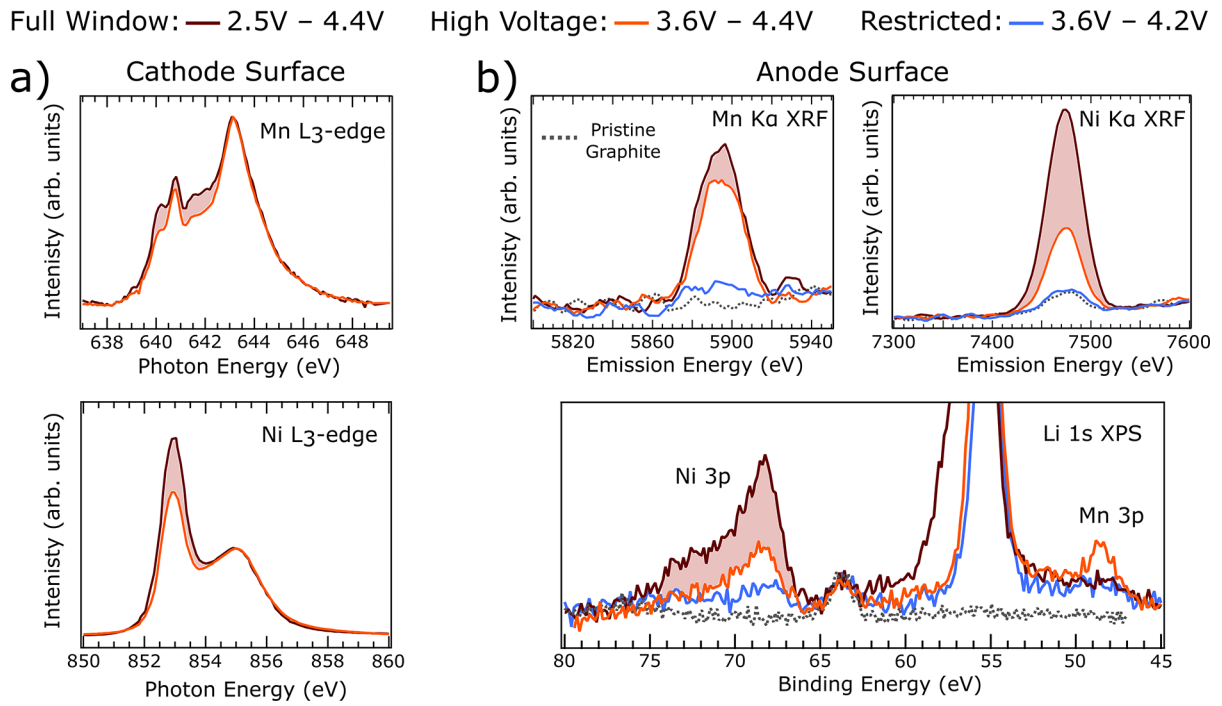

Figure 4. (a) Soft XAS experiments on the cathode electrode using Mn L-edge and Ni L-edge XAS. (b) Cross-talk analysis with XPS and XRF on the graphite electrodes showing a correlation between the surface reduction and transition metal dissolution/deposition

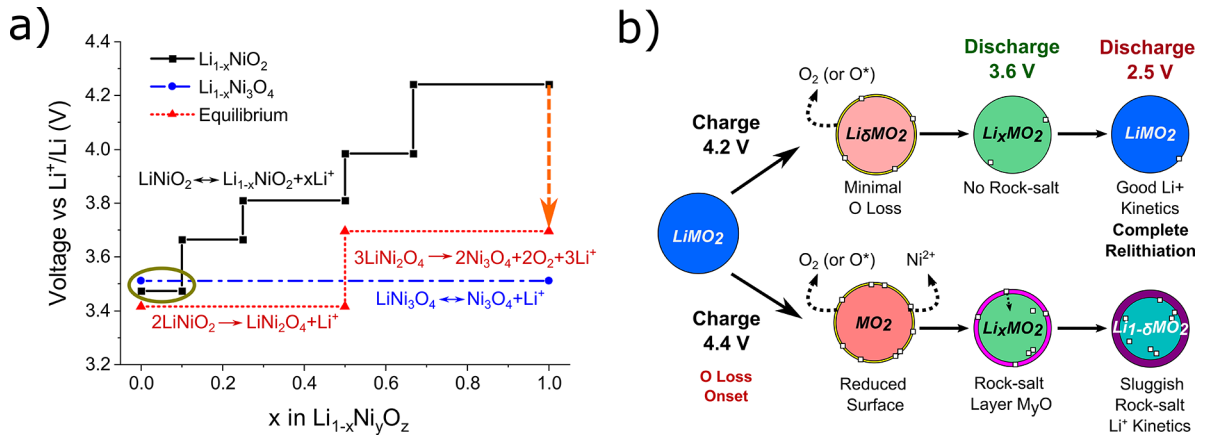

Figure 5. (a) Voltage vs degree of lithiation in $Li_{1-x}NiO_2$ predicted from DFT calculations. Black curve: layered $Li_{1-x}NiO_2$ structures. Red dotted curve: structural transformations between layered $LiNiO_2$, spinel ($LiNi_2O_4$), and rocksalt like (Ni_3O_4) structures. Blue dot-dash curve: lithiation of the rocksalt like $Li_{1-x}Ni_3O_4$ structure. Orange arrow: voltage difference between the layered structure pathway and the equilibrium pathway. Gold oval: The lithiation of the Ni_3O_4 phase is thermodynamically more favorable than the layered $Li_{1-x}NiO_2$ phase. (b) Schematic representation of the underlying mechanism governing the synergistic degradation.

Restricted and the High Voltage protocols. Only for the Full Window protocol does the P_4 reveal a certain degree of structural impact, indicating less *c*-lattice activity within the structure. The reduction in the *c*-lattice activity could stem from some unit cells arbitrarily changing into a locally (short-range) less redox-active phase. The local changes may expand with the number of cycles and become XRD detectable in the long term, as observed in the literature as a gradually invariant *c*-lattice.[21,27] The emergence of this inactive phase can lead to increasing crystal heterogeneity, which can impact the Li-ion kinetics in the long term.[27] Additionally, Figure 3b shows there is negligible cracking after the cycling protocols, with statistically robust evidence provided in Figure S4, ruling out material surface changes to stem from severe particle cracking as observed in other systems[28] and primarily be related with the synergistic mechanism discussed below.

To examine the evolution of the cathode electrolyte interface (CEI) upon surface O loss and DoD, we employ a combination of X-ray spectroscopy techniques. With a 4.4 V UCV, the Full Window protocol results in a CEI of 2.78 nm in thickness from O 1s HAXPES analysis compared to the 1.11 nm CEI thickness at 3.6 V DoD (section S5), providing further evidence of DoD densification. With a typical probing depth of >2.78 nm, soft X-ray absorption spectroscopy (XAS) can test reduced (i.e., NiO-like) surface phases and the underlying subsurface structure of redox-active Ni-rich NMC. Given the cells are at the same discharge state, we normalize the XAS spectra to the electrochemically active peaks (643 and 855 eV

https://doi.org/10.1021/acsenergylett.3c01596
ACS Energy Lett. 2023, 8, 5025−5031

peak in the Mn L-edge and Ni L-edge, respectively) so that surface evolution is easily observed from changes at 641 eV in Mn L-edge and 853 eV in Ni L-edge (Figure 4).

The SC Ni-rich material contains Al surface dopants (Figure S5), proven to suppress surface degradation when cycled slightly below the oxygen loss threshold.[16] In contrast, above this point (i.e., with a 4.4 V UCV, Full Window and High Voltage protocols) the surface evolution is dictated by the synergistic degradation. The shaded region in Figure 4a indicates that the Full Window protocol leads to larger surface reconstruction activity, indicating that the oxygen vacancies formed at high voltages tend to densify into reduced surface phases at deeper DoD, consistent with prior findings from STEM-EELS.[3] The densified layer results from the larger mobility of the oxygen vacancies at deeper DoD. These findings pair with an increasing anode cross-talk activity observed in Figure 4b. The amount of transition metal (TM) species deposited on the graphite (Restricted < High Voltage < Full Window) correlates with the surface reconstruction activities at the cathode side. X-ray fluorescence (XRF) and X-ray photoelectron spectroscopy (XPS) show a moderate increase between the Restricted and the High Voltage regime. Nonetheless, intensities for Ni triple after the Full Window cycling due to the synergistic degradation. The reconstruction and densification of the NMC surface layer during the Full Window cycling promote larger amounts of densified Ni oxides to dissolve. Note however that the amount of TM dissolution is more than an order of magnitude less than that for PC Ni-rich NMC//graphite under the same conditions (Figure S6); therefore it is proposed that kinetic issues associated with the reduced surface evolution are the main factor responsible for capacity fading.

Density functional theory (DFT) studies using energetics from the Materials Project database[29] (Table S1) on layered $LiNiO_2$, $LiNi_2O_4$, rocksalt (NiO), and rocksalt like (Ni_3O_4)[30] as model systems are a reliable tool to identify the driving forces for synergistic degradation observed after cycling with the Full Window protocol.

During charging, the delithiation pathway of the layered $Li_{1-x}NiO_2$ structure is shown in black in Figure 5a. Li deintercalation starts at 3.47 V (vs Li metal) to $Li_{0.9}NiO_2$. Further Li removal occurs with $Li_{1-x}NiO_2$ structures at 3.66, 3.81, and 3.98 V for x = 0.25, 0.5, and 0.67, respectively. Removal of the final third of the Li from the layered structure for $x = 0.67 \rightarrow 1$ occurs at $V > 4.24$ V, near the measured oxygen loss threshold and in accordance with other works.[31] However, this deintercalation mechanism from the layer $LiNiO_2$ structure results in a sequence of metastable layered Li_xNiO_2 phases. The thermodynamically favored route has a markedly different energy as shown by the red curve in Figure 5a. Under thermodynamic equilibrium the $LiNi_2O_4$ spinel structure at 3.42 V is more stable so that at x = 0.5, a driving force of −41 meV/atom would transform layered $Li_{0.5}NiO_2$ structure into the spinel phase.[32]

On full delithiation, NiO_2 is metastable relative to the "rocksalt-like" Ni_3O_4 phase generating O_2 gas via

$$3NiO_2 \rightarrow Ni_3O_4 + O_2$$

with a very strong driving force of −127 meV/atom at 0 K, as shown by the orange line arrow in Figure 5a. A second reaction of a fully dense reduced NiO rocksalt phase, $3NiO_2 \rightarrow 3NiO + {}^3/_2O_2$ is also possible at 0 K (Figure S7) with a relatively smaller driving force at −107 meV/atom. This secondary reaction becomes favorable at ambient conditions in the presence of ethylene carbonate (EC) in the electrolyte which respectively reduces the oxygen chemical potential μ_O (<−4.982 eV) (section S7).

During the discharge stage, reinsertion of Li can occur into the remaining NiO_2 in addition to the newly formed rocksalt like Ni_3O_4 phase on the particle surface. Due to the ordered arrangement of Ni^{2+} and Ni^{4+} chains in Ni_3O_4,[30] Li can be inserted into the 1D tunnels within the structure, spending less energy compared to the other phases (blue curve in Figure 5a). Relithiation of the Ni_3O_4 phase occurs at 3.51 V. When the NMC potential in the cycling protocols is below 3.51 V vs Li/Li^+ (theory), the Li sites within the $LiNi_3O_4$ structure are fully occupied, and Li transport through this surface layer and into the layered $Li_{1-x}NiO_2$ bulk structure on further discharge must be sluggish. As more of this reduced phase is formed during cycling, we expect that the slow lithium mobility leads to an increased population of trapped lithium and hence capacity loss. Thus, the formation of a (Li)Ni_3O_4 surface phase results from cycling to high and low voltages.

A schematic in Figure 5b summarizes the stages of the underlying mechanism for synergistic degradation, supported by experimental findings and DFT, and explains the observed phenomena. With V greater than the oxygen loss onset, the oxygen vacancies lead to dense regions with reduced surface phases upon deeper DoD. Meanwhile, avoiding accessing the oxygen loss threshold prevents the NMC surface from developing surface phases that limit the Li kinetics.

In conclusion, we have observed synergistic degradation and isolated the contributions to this effect in SC $LiNi_{0.834}Mn_{0.095}Co_{0.071}O_2$//graphite pouch cells using carefully designed cycling protocols. The mechanism governing the synergistic degradation consists of two parts: first, at high voltages (>4.33 V vs Li/Li^+) the formation of cathode surface oxygen vacancies is promoted at the Ni-rich/electrolyte interface, where surface reconstruction and EC decomposition pathways force $NiO_2 \rightarrow Ni_3O_4$ and NiO.

Second, the improved kinetics of oxygen vacancies with increased depth of discharge results in the formation of densified reduced surface phases that present additional kinetic barriers for Li-ion diffusion (i.e., trapped lithium). As a result, the choice of the high- and low-voltage cutoffs ultimately dictates the cell longevity. While demonstrated here for NMC 811 cathode chemistry, we expect this synergistic mechanism to be universal for NMC//graphite systems when operating at regimes to induce oxygen loss (regardless of Ni content). Furthermore, it should also be apparent in next-generation chemistries such as Li-excess/SiO_x-graphite systems.

■ ASSOCIATED CONTENT

Supporting Information

The Supporting Information is available free of charge at https://pubs.acs.org/doi/10.1021/acsenergylett.3c01596.

Methodology and details on cells and active materials, normalized capacity graph to show SEI dominated degradation, dQ/dV and the crystal structure, SEM Ni-rich single crystal particle morphology, CEI and surface species, cross-talk PC vs SC, and model for interpreting the high and low degradation (PDF)

https://doi.org/10.1021/acsenergylett.3c01596
ACS Energy Lett. 2023, 8, 5025−5031

AUTHOR INFORMATION

Corresponding Authors

Galo J. Páez Fajardo − *WMG, University of Warwick, Coventry CV4 7AL, United Kingdom; The Faraday Institution, Didcot OX11 0RA, United Kingdom;* orcid.org/0000-0003-0639-2896; Email: galo.paez-fajardo@warwick.ac.uk

Louis F. J. Piper − *WMG, University of Warwick, Coventry CV4 7AL, United Kingdom; The Faraday Institution, Didcot OX11 0RA, United Kingdom;* orcid.org/0000-0002-3421-3210; Email: louis.piper@warwick.ac.uk

Authors

Eleni Fiamegkou − *WMG, University of Warwick, Coventry CV4 7AL, United Kingdom; The Faraday Institution, Didcot OX11 0RA, United Kingdom*

James A. Gott − *WMG, University of Warwick, Coventry CV4 7AL, United Kingdom*

Heng Wang − *Department of Engineering, Institute for Manufacturing, University of Cambridge, Cambridge CB3 0FS, United Kingdom; The Faraday Institution, Didcot OX11 0RA, United Kingdom*

Israel Temprano − *Yusuf Hamied Department of Chemistry, University of Cambridge, Cambridge CB2 1EW, United Kingdom; The Faraday Institution, Didcot OX11 0RA, United Kingdom*

Ieuan D. Seymour − *Department of Chemistry, University of Aberdeen, Aberdeen AB24 3UE, United Kingdom; Department of Materials, Imperial College London, London SW7 2AZ, United Kingdom; Advanced Centre for Energy and Sustainability (ACES), Department of Chemistry, University of Aberdeen, Aberdeen AB24 3UE Scotland, United Kingdom; The Faraday Institution, Didcot OX11 0RA, United Kingdom;* orcid.org/0000-0002-9550-9971

Matthew J. W. Ogley − *WMG, University of Warwick, Coventry CV4 7AL, United Kingdom; The Faraday Institution, Didcot OX11 0RA, United Kingdom*

Ashok S. Menon − *WMG, University of Warwick, Coventry CV4 7AL, United Kingdom; The Faraday Institution, Didcot OX11 0RA, United Kingdom*

Ifan E. L. Stephens − *Department of Materials, Imperial College London, London SW7 2AZ, United Kingdom;* orcid.org/0000-0003-2157-492X

Muhammad Ans − *WMG, University of Warwick, Coventry CV4 7AL, United Kingdom; The Faraday Institution, Didcot OX11 0RA, United Kingdom*

Tien-Lin Lee − *Diamond Light Source, Didcot OX11 0DE, United Kingdom*

Pardeep K. Thakur − *Diamond Light Source, Didcot OX11 0DE, United Kingdom;* orcid.org/0000-0002-9599-0531

Wesley M. Dose − *School of Chemistry, The University of New South Wales, Sydney, NSW 2052, Australia;* orcid.org/0000-0003-3850-0505

Michaël F. L. De Volder − *Department of Engineering, Institute for Manufacturing, University of Cambridge, Cambridge CB3 0FS, United Kingdom; The Faraday Institution, Didcot OX11 0RA, United Kingdom*

Clare P. Grey − *Yusuf Hamied Department of Chemistry, University of Cambridge, Cambridge CB2 1EW, United Kingdom; The Faraday Institution, Didcot OX11 0RA, United Kingdom;* orcid.org/0000-0001-5572-192X

Complete contact information is available at: https://pubs.acs.org/10.1021/acsenergylett.3c01596

Notes

The authors declare no competing financial interest.

ACKNOWLEDGMENTS

We acknowledge Diamond Light Source for time on beamline I09 under Proposals SI30201-1 and SI30201-2. This work is supported by the Faraday Institution under Grants FIRG044, FIRG024, and FIRG060.

REFERENCES

(1) Reniers, J. M.; Mulder, G.; Howey, D. A. Review and Performance Comparison of Mechanical-Chemical Degradation Models for Lithium-Ion Batteries. *J. Electrochem. Soc.* **2019**, *166*, A3189.

(2) Dose, W. M.; Xu, C.; Grey, C. P.; De Volder, M. F. L. Effect of Anode Slippage on Cathode Cutoff Potential and Degradation Mechanisms in Ni-Rich Li-Ion Batteries. *Cell Reports Physical Science* **2020**, *1*, 100253.

(3) Dose, W. M.; Morzy, J. K.; Mahadevegowda, A.; Ducati, C.; Grey, C. P.; De Volder, M. F. L. The influence of electrochemical cycling protocols on capacity loss in nickel-rich lithium-ion batteries. *J. Mater. Chem. A* **2021**, *9*, 23582−23596.

(4) Eldesoky, A.; Bauer, M.; Bond, T.; Kowalski, N.; Corsten, J.; Rathore, D.; Dressler, R.; Dahn, J. R. Long-Term Study on the Impact of Depth of Discharge, C-Rate, Voltage, and Temperature on the Lifetime of Single-Crystal NMC811/Artificial Graphite Pouch Cells. *J. Electrochem. Soc.* **2022**, *169*, 100531.

(5) Zhang, H.; Liu, H.; Piper, L. F. J.; Whittingham, M. S.; Zhou, G. Oxygen Loss in Layered Oxide Cathodes for Li-Ion Batteries: Mechanisms, Effects, and Mitigation. *Chem. Rev.* **2022**, *122*, 5641−5681.

(6) Dose, W. M.; Li, W.; Temprano, I.; O'Keefe, C. A.; Mehdi, B. L.; De Volder, M. F. L.; Grey, C. P. Onset Potential for Electrolyte Oxidation and Ni-Rich Cathode Degradation in Lithium-Ion Batteries. *ACS Energy Letters* **2022**, *7*, 3524−3530.

(7) Kim, T. Voltage-dependent formation of cathode−electrolyte interphase with independent metallic layer in $LiNi_{0.8}Mn_{0.1}Co_{0.1}O_2$ cathode for high-energy density lithium-ion batteries. *Materials Today Sustainability* **2023**, *21*, 100326.

(8) Grey, C. P.; Hall, D. S. Prospects for lithium-ion batteries and beyond—a 2030 vision. *Nat. Commun.* **2020**, *11*, 6279.

(9) Kim, M.-H.; Shin, H.-S.; Shin, D.; Sun, Y.-K. Synthesis and electrochemical properties of $Li[Ni_{0.8}Co_{0.1}Mn_{0.1}]O_2$ and $Li[Ni_{0.8}Co_{0.2}]O_2$ via co-precipitation. *J. Power Sources* **2006**, *159*, 1328−1333.

(10) Sun, H.-H.; Choi, W.; Lee, J. K.; Oh, I.-H.; Jung, H.-G. Control of electrochemical properties of nickel-rich layered cathode materials for lithium ion batteries by variation of the manganese to cobalt ratio. *J. Power Sources* **2015**, *275*, 877−883.

(11) Yoon, C. S.; Choi, M. H.; Lim, B.-B.; Lee, E.-J.; Sun, Y.-K. Review—High-Capacity $Li[Ni_{1-x}Co_{x/2}Mn_{x/2}]O_2$ (x = 0.1, 0.05, 0) Cathodes for Next-Generation Li-Ion Battery. *J. Electrochem. Soc.* **2015**, *162*, A2483.

(12) Li, J.; Downie, L. E.; Ma, L.; Qiu, W.; Dahn, J. R. Study of the Failure Mechanisms of $LiNi_{0.8}Mn_{0.1}Co_{0.1}O_2$ Cathode Material for Lithium Ion Batteries. *J. Electrochem. Soc.* **2015**, *162*, A1401.

(13) Harlow, J. E.; Ma, X.; Li, J.; Logan, E.; Liu, Y.; Zhang, N.; Ma, L.; Glazier, S. L.; Cormier, M. M. E.; Genovese, M.; Buteau, S.; Cameron, A.; Stark, J. E.; Dahn, J. R. A Wide Range of Testing Results on an Excellent Lithium-Ion Cell Chemistry to be used as Benchmarks for New Battery Technologies. *J. Electrochem. Soc.* **2019**, *166*, A3031.

(14) Wandt, J.; Freiberg, A. T.; Ogrodnik, A.; Gasteiger, H. A. Singlet oxygen evolution from layered transition metal oxide cathode materials and its implications for lithium-ion batteries. *Mater. Today* **2018**, *21*, 825−833.

(15) Zhou, H.; Xin, F.; Pei, B.; Whittingham, M. S. What Limits the Capacity of Layered Oxide Cathodes in Lithium Batteries? *ACS Energy Letters* **2019**, *4*, 1902−1906.
(16) Páez Fajardo, G. J.; et al. Understanding improved capacity retention at 4.3 V in modified single crystal Ni-rich NMC//graphite pouch cells at elevated temperature. *RSC Appl. Interfaces* **2023**, DOI: 10.1039/D3LF00093A.
(17) Märker, K.; Reeves, P. J.; Xu, C.; Griffith, K. J.; Grey, C. P. Evolution of Structure and Lithium Dynamics in $LiNi_{0.8}Mn_{0.1}Co_{0.1}O_2$(NMC 811) Cathodes during Electrochemical Cycling. *Chem. Mater.* **2019**, *31*, 2545−2554.
(18) Jung, R.; Metzger, M.; Maglia, F.; Stinner, C.; Gasteiger, H. A. Chemical versus Electrochemical Electrolyte Oxidation on NMC111, NMC22, NMC11, LNMO, and Conductive Carbon. *J. Phys. Chem. Lett.* **2017**, *8*, 4820−4825.
(19) Jung, R.; Metzger, M.; Maglia, F.; Stinner, C.; Gasteiger, H. A. Oxygen Release and Its Effect on the Cycling Stability of $LiNi_x$ Mn_y Co_z O_2 (NMC) Cathode Materials for Li-Ion Batteries. *J. Electrochem. Soc.* **2017**, *164*, A1361.
(20) Louli, A. J.; Li, J.; Trussler, S.; Fell, C. R.; Dahn, J. R. Volume, Pressure and Thickness Evolution of Li-Ion Pouch Cells with Silicon-Composite Negative Electrodes. *J. Electrochem. Soc.* **2017**, *164*, A2689.
(21) Menon, A. S.; Shah, N.; Gott, J. A.; Fiamegkou, E.; Ogley, M. J. W.; Fajardo, G. J. P.; Vaenas, N.; Ellis, I.; Malliband, P.; West, G.; Walker, D.; Loveridge, M.; Piper, L. Operando X-ray and Post-mortem Investigations of Electrochemical Degradation in Single-crystalline $LiNi_{0.8}Mn_{0.1}Co_{0.1}O_2$−Graphite pouch cells. *ChemRxiv* **2023**, DOI: 10.26434/chemrxiv-2023-zs9kp.
(22) Gauthier, R.; Luscombe, A.; Bond, T.; Bauer, M.; Johnson, M.; Harlow, J.; Louli, A. J.; Dahn, J. R. How do Depth of Discharge, C-rate and Calendar Age Affect Capacity Retention, Impedance Growth, the Electrodes, and the Electrolyte in Li-Ion Cells? *J. Electrochem. Soc.* **2022**, *169*, No. 020518.
(23) Sun, J.; Cao, X.; Yang, H.; He, P.; Dato, M. A.; Cabana, J.; Zhou, H. The Origin of High-Voltage Stability in Single-Crystal Layered Ni-Rich Cathode Materials. *Angew. Chem., Int. Ed.* **2022**, *61*, No. e202207225.
(24) Park, N.-Y.; Park, G.-T.; Kim, S.-B.; Jung, W.; Park, B.-C.; Sun, Y.-K. Degradation Mechanism of Ni-Rich Cathode Materials: Focusing on Particle Interior. *ACS Energy Letters* **2022**, *7*, 2362−2369.
(25) Ruff, Z.; Coates, C. S.; Märker, K.; Mahadevegowda, A.; Xu, C.; Penrod, M. E.; Ducati, C.; Grey, C. P. O3 to O1 Phase Transitions in Highly Delithiated NMC811 at Elevated Temperatures. *Chem. Mater.* **2023**, *35*, 4979−4987.
(26) Kondrakov, A. O.; Geßwein, H.; Galdina, K.; de Biasi, L.; Meded, V.; Filatova, E. O.; Schumacher, G.; Wenzel, W.; Hartmann, P.; Brezesinski, T.; Janek, J. Charge-Transfer-Induced Lattice Collapse in Ni-Rich NMCCathode Materials during Delithiation. *J. Phys. Chem. C* **2017**, *121*, 24381−24388.
(27) Xu, C.; Märker, K.; Lee, J.; Mahadevegowda, A.; Reeves, P. J.; Day, S. J.; Groh, M. F.; Emge, S. P.; Ducati, C.; Layla Mehdi, B.; Tang, C. C.; Grey, C. P. Bulk fatigue induced by surface reconstruction in layered Ni-rich cathodes for Li-ion batteries. *Nat. Mater.* **2021**, *20*, 84−92.
(28) Björklund, E.; Xu, C.; Dose, W. M.; Sole, C. G.; Thakur, P. K.; Lee, T.-L.; De Volder, M. F. L.; Grey, C. P.; Weatherup, R. S. Cycle-Induced Interfacial Degradation and Transition-Metal Cross-Over in $LiNi_{0.8}Co_{0.1}Mn_{0.1}O_2$−Graphite Cells. *Chem. Mater.* **2022**, *34*, 2034−2048.
(29) Jain, A.; Ong, S. P.; Hautier, G.; Chen, W.; Richards, W. D.; Dacek, S.; Cholia, S.; Gunter, D.; Skinner, D.; Ceder, G.; Persson, K. A. The Materials Project: A materials genome approach to accelerating materials innovation. *APL Mater.* **2013**, *1*, No. 011002.
(30) Das, H.; Urban, A.; Huang, W.; Ceder, G. First-Principles Simulation of the (Li−Ni−Vacancy)O Phase Diagram and Its Relevance for the Surface Phases in Ni-Rich Li-Ion Cathode Materials. *Chem. Mater.* **2017**, *29*, 7840−7851.
(31) Xu, C.; Merryweather, A. J.; Pandurangi, S. S.; Lun, Z.; Hall, D. S.; Deshpande, V. S.; Fleck, N. A.; Schnedermann, C.; Rao, A.; Grey, C. P. Operando visualization of kinetically induced lithium heterogeneities in single-particle layered Ni-rich cathodes. *Joule* **2022**, *6*, 2535−2546.
(32) Xiao, P.; Shi, T.; Huang, W.; Ceder, G. Understanding Surface Densified Phases in Ni-Rich Layered Compounds. *ACS Energy Letters* **2019**, *4*, 811−818.

NOTE ADDED AFTER ASAP PUBLICATION

This paper was published ASAP on November 6, 2023, with an error in Figure 5. The corrected version was reposted on November 8, 2023.

https://doi.org/10.1021/acsenergylett.3c01596
ACS Energy Lett. 2023, 8, 5025−5031